Turbulence anisotropy and the SO(3) description

Adrian Staicu, Bart Vorselaars, and Willem van de Water

Physics Department, Eindhoven University of Technology, Postbus 513, 5600 MB Eindhoven, The Netherlands

We study strongly turbulent windtunnel flows with controlled anisotropy. Using a recent formalism based on angular momentum and the irreducible representations of the SO(3) rotation group, we attempt to extract this anisotropy from the angular dependence of second-order structure functions. Our instrumentation allows a measurement of both the separation and the angle dependence of the structure function. In axisymmetric turbulence which has a weak anisotropy, this more extended information produces ambiguous results. In more strongly anisotropic shear turbulence, the SO(3) description enables one to find the anisotropy scaling exponent. The key quality of the SO(3) description is that structure functions are a mixture of algebraic functions of the scale with exponents ordered such that the contribution of anisotropies diminishes at small scales. However, we find that in third-order structure functions of homogeneous shear turbulence the anisotropic contribution is always large and of the same order of magnitude as the isotropic part. Our results concern the minimum instrumentation needed to determine the parameters of the SO(3) description, and raise several questions about its ability to describe the angle dependence of high-order structure functions.

I. INTRODUCTION

Angular momentum theory has provided a new and interesting way to describe anisotropic turbulence [1,2]. Although the idea was proposed earlier [3] and expansion of tensorial quantities using the irreducible representations of the rotation group is well known [4], the current interest is in scaling properties of anisotropic turbulence quantities, such that each irreducible representation is expected to have its own (universal) scaling exponent. These phenomena become accessible in experiments which go beyond the traditional measurement of a single velocity component at a single point in strongly turbulent flows [5,6].

The idea is that the Navier-Stokes equation is invariant under rotations of space, and, therefore, that statistical turbulence quantities should be expanded preferably in terms of the irreducible representations of the rotation group. In angular momentum theory there is a relation between the value of the angular momentum and the irreducible representation of the rotation group, such that a higher angular momentum signifies less symmetry. This provides a way to describe the influence of anisotropy on turbulence by the gradual loss of symmetry of turbulence statistical quantities at increasing length scales, and accordingly, an increasing influence of high angular momentum contributions.

As most turbulent flows in the laboratory are anisotropic, and as it has recently become clear that this anisotropy most probably remains, even at the smallest scales [7,8], this new description of anisotropy is a very significant development which deserves a careful experimental test. The goal of this paper is to provide such a test by devising experimental techniques in turbulent flows which have a controlled anisotropy.

In order to illustrate this idea, we consider the structure functions

$$G_{\alpha\beta}(\boldsymbol{r}) = \langle [u_\alpha(\boldsymbol{x}+\boldsymbol{r})-u_\alpha(\boldsymbol{x})][u_\beta(\boldsymbol{x}+\boldsymbol{r})-u_\beta(\boldsymbol{x})]\rangle, \quad (1)$$

which involve increments of the velocity components u_α and

u_β over the separation vector $\boldsymbol{r}$. The ensemble average is denoted by $\langle\cdots\rangle$; homogeneity of the flow implies independence of $\boldsymbol{x}$. Adopting a coordinate system in which we measure the x component of the velocity and where the spherical coordinates (r,θ,ϕ) are defined with respect to the x axis as polar axis, the angular momentum decomposition of the tensor, Eq. (1) takes on the following form:

$$G_{xx}(r,\theta,\phi) = g_{l=0}(\theta)r^{\zeta_2^{(0)}} + g_{l=2}(\theta,\phi)r^{\zeta_2^{(2)}} + \cdots, \quad (2)$$

where the first term is the isotropic contribution and the term involving g_2 is the first anisotropic part, possibly followed by terms representing higher-order anisotropies. The angle-dependent functions g_l are subject to the incompressibility constraint which determines $g_0(\theta)$ upto a constant factor. Parity invariance prevents a contribution with $l=1$. As is implied by Eq. (2), each irreducible part may have its own scaling exponent, so that $\zeta_2^{(0)}$, $\zeta_2^{(2)}$, ... may all be different. Of course, any tensorial quantity can be expanded in irreducible components of the rotation group [4], but the separation of G_{xx} into angle-dependent factors which multiply algebraic (scaling) functions of r is new. Whilst $g_l(\theta,\phi)$ coincide with the orthogonal spherical harmonics for a scalar field and for the longitudinal correlations of the velocity field (where the measured velocity component and $\boldsymbol{r}$ point in the same direction), they have a more complicated form in the general case. However, this form can be readily derived using the well-known tools from angular momentum theory in quantum mechanics. Often, the irreducible representations are called "sectors," with the first term of Eq. (2) belonging to the isotropic sector, and the second term belonging to the first anisotropic sector.

Unlike the nonrelativistic Schrödinger equation which is linear, the Navier-Stokes equation is nonlinear and the expansion, Eq. (2), is only appropriate if the anisotropic contributions take the form of small perturbations whose sizes rapidly decrease with increasing l. Accordingly, the expo-

nents associated with increasing angular momentum are ordered hierarchically, $\zeta_2^{(0)} < \zeta_2^{(2)} < \cdots$, such that the highest angular momentum contribution decays quickest at decreasing scale r.

Two special forms of $G_{\alpha\beta}(r)$ are the transverse structure function $G_2^T(r) \equiv G_{\alpha\alpha}(re_\beta)$, with $\alpha \neq \beta$ and e_α being the unit vector in the α direction, and the longitudinal structure function $G^L(r) \equiv G_{\alpha\alpha}(re_\alpha)$. With $\alpha = x$ and $\beta = y$ we pointed out that the high-order longitudinal and transverse structure functions may have different scaling exponents [9,10]. This was also found in other experiments [11] and direct numerical simulations [12–14], but Shen and Warhaft [15] have suggested that this difference disappears at large Reynolds numbers. It must be realized that a dependence of the scaling exponent on the relative orientation of r and the direction of the measured velocity component is *incompatible* with the description [Eq. (2)] in terms of irreducible components. In this description, it is neither the longitudinal nor the transverse structure functions that carry the pure scaling, but rather the different terms of the angular momentum decomposition Eq. (2). However, the irreducible constituents of the longitudinal and transverse structure functions may conspire such that at *finite* Reynolds numbers, the longitudinal and transverse structure functions may have different *apparent* scaling exponents, with their mixed character only emerging at Reynolds numbers that are unreachable in the experiment. An example of this was given in Ref. [16].

In the SO(3) picture, all structure functions $G_{\alpha\beta}(r)$ embody a mixture of scalings, with the pure algebraic behavior carried by the irreducible components. In other words, if it is possible to single out these components, a much improved scaling behavior of measured structure functions would be the result in cases where the large-scale anisotropies invade the inertial-range scales, that is, at small Reynolds numbers [17]. Such an approach can only be followed in numerical simulations where the full vector information about the velocity field is available.

In case of the longitudinal structure functions $G_2^L(r)$, the SO(3) representations $g_l(\theta, \phi)$ coincide with the spherical harmonics, where its arguments θ, ϕ are the angles of the vector r in $G_2^L(r) = \langle [\hat{r} \cdot (u(x+r) - u(x))]^2 \rangle$. By projecting onto the spherical harmonics Biferale and Toschi [18] have singled out the isotropic component of longitudinal structure functions of a numerically computed velocity field and demonstrated its superior scaling behavior compared to the ordinary, unfiltered second-order structure function. However, the computed flow was driven strongly inhomogeneously with homogeneity recovered only in a statistical sense. Further, Biferale and Toschi [18] do not report scaling behavior of the ordinary third-order longitudinal structure function, and the Reynolds number was not known, possibly because of the used hyperviscosity.

Experiments can reach much larger Reynolds numbers than numerical simulations and can average over many large-eddy turnover times. At large Reynolds numbers, there is a clear separation between the inertial-range scales and the scales which are invaded by anisotropies, which may facilitate the analysis. Also, experiments allow a precise control

over homogeneity and anisotropy using active [7] or passive grids to stir the flow. However, experiments have limited access to the velocity field: hot-wire velocimetry provides only a few velocity components in a few spatial points. In the context of experiments, therefore, the question is if the mixture of scaling exponents of Eq. (2) gives a better description of measured structure functions than a pure algebraic behavior. Such a mixture then must exhibit the angular dependence that is characteristic of the SO(3) description.

The functional form of the irreducible components $g_l(\theta, \phi)$, $l \geq 2$, depends on the symmetry of the experiment and is determined by parameters that are specific for the kind of flow. With decreasing symmetry, the number of parameters increases. However, the value of the *exponents* $\zeta_2^{(l)}$ is expected to be universal. For example, a simple dimensional argument [19] predicts $\zeta_2^{(2)} = 4/3$ for the first anisotropy exponent.

In an experiment one must try to determine both the universal exponents and the nonuniversal constants that parametrize the angle dependent $g_2(\theta, \phi)$. The large number of adjustable parameters is a problem: With so much freedom it is often not difficult to obtain a better fit of the data and it becomes unclear if an improved fit is the consequence of the specific anisotropy description Eq. (2), or of the large number of adjustable constants. In this paper we will design experiments such as to actually *minimize* the number of constants, and simultaneously *maximize* the experimental information.

II. ANGULAR DEPENDENCE OF STRUCTURE FUNCTIONS

Clearly, experiments must now measure both the r and the angle (θ, ϕ) dependence of the structure functions, which calls for more sophisticated setups than the common single point, single-velocity component experiments that give access to the longitudinal structure function only. Using multiple-velocity probes that measure a single velocity component, Fig. 1 sketches two ways to measure both r and θ dependence of the structure function. The idea is to combine true spatial separations with temporal delays, which in turn translate into spatial separations using the Taylor frozen turbulence hypothesis. In the first manner [method (i)], exploited in Refs. [2,6], both r and θ dependencies are measured simultaneously by time-delaying the signal of one of the two probes used. If the frozen turbulence hypothesis holds, the angle θ is given by $\theta(r) = \sin^{-1}(r_0/r)$, with $r^2 = r_0^2 + (U\tau)^2$, where U is the mean velocity and τ is the time delay.

By using arrays of many probes [method (ii)], Fig. 1(b) illustrates that it is possible to measure the r and θ dependence of structure functions separately. Obviously, method (i) provides quite limited information about the structure function. The information gained about the anisotropic velocity field in method (ii) is one of the key points of this paper.

Using straightforward angular momentum theory (Clebsch-Gordan algebra) [2], it is possible to arrive at explicit expressions for the irreducible components $g_l(\theta, \phi)$ of
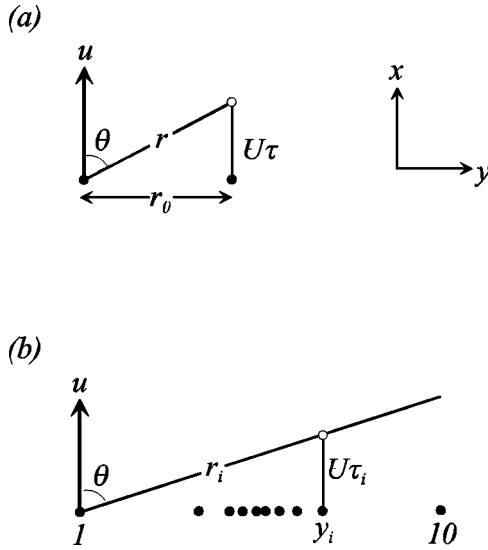
FIG. 1. Probe geometries for measuring both r and θ dependence of structure functions. (a) With two probes, r and θ are related through the time delay τ, $\theta = \tan^{-1}(r_0/U\tau)$, $r^2 = r_0^2 + (U\tau)^2$. (b) With ten probes, r spans 45 discrete values, and θ can be varied independently by selecting time delays $\tau_i = y_i/(U\tan\theta)$.

the second-order structure function. Here, it suffices to list the result for flows with decreasing symmetry. We will specialize the formulas for our case, in which we measure the x component of the fluctuating velocity in axisymmetric and shear turbulence. In both cases the flow is assumed homogeneous. The used coordinate system is sketched in Fig. 2.

In the case of *axisymmetric* turbulence, all statistical quantities are invariant under rotations around the x axis, that is, $G_{xx}(r,\theta,\phi)$ becomes independent of ϕ,

$$G_{xx}(r,\theta) = g_0(\theta)r^{\zeta_2^{(0)}} + g_2(\theta)r^{\zeta_2^{(2)}}$$

$$= c_0\{2 + \zeta_2^{(0)}\sin^2\theta\}r^{\zeta_2^{(0)}} + \{d_1 + d_2\cos(2\theta)$$

$$+ \kappa(d_1,d_2,\zeta_2^{(2)})\cos(4\theta)\}r^{\zeta_2^{(2)}}, \qquad (3)$$

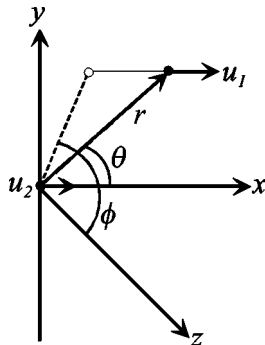with the function κ determined by axisymmetry,

FIG. 2. Coordinate system: velocity increments $u_1 - u_2$ are measured over a vector $\mathbf{r}$ with the measured velocity component pointing in the $\mathbf{e}_x$ direction.

$$\kappa(d_1,d_2,\zeta_2^{(2)}) = \frac{[2 - \zeta_2^{(2)}][\zeta_2^{(2)}d_1 + (4 + \zeta_2^{(2)})d_2]}{[\zeta_2^{(2)} + 7 + \sqrt{17}][\zeta_2^{(2)} + 7 - \sqrt{17}]}.$$

As is well known, the isotropic part involves $\sin^2\theta$, with the explicit form of $g_0(\theta)$ set by incompressibility.

In the case of shear turbulence, the velocity gradient points in the y direction. In this case we have the reflection symmetry $G_{xx}(r,\theta,\phi) = G_{xx}(r,\theta,\pi-\phi)$. At $\phi=0$ the partial symmetry $G_{xx}(r,\theta,\phi=0) = G_{xx}(r,\pi-\theta,\phi=0)$ leads to the following expression for the anisotropic contribution:

$$g_2(\theta) = d_1 + d_2\cos(2\theta) + d_3\cos(4\theta), \qquad (4)$$

where the parameters $d_{1,2}$ are different from the parameters with the same name in Eq. (3). The loss of axisymmetry results in an extra free parameter d_3. At azimuthal angles away from $\phi=0$, the anisotropic contribution acquires another free parameter and becomes

$$g_2(\theta) = d_1 + d_2\cos(2\theta) + d_3\cos(4\theta)$$

$$+ d_4[(12 + 2\zeta_2^{(2)})\sin(2\theta) + (2 - \zeta_2^{(2)})\sin(4\theta)], \qquad (5)$$

whereas the ϕ dependence is given by

$$g_2(\phi) = d_5 + d_6\cos(2\phi), \qquad (6)$$

where in Eqs. (5) and (6) the parameters $d_{1,2,3}$ are different from the parameters with the same name in earlier expressions. Because Eqs. (5) and (6) involve disjunct sets of parameters, it is not possible to reconstruct the ϕ dependence of g_2 at a given angle θ from its θ dependence at a given ϕ. Equations (4) and (5) are completely equivalent to those in Ref. [6], but we point out that Eq. (13) of Ref. [6] is in error because it contains a redundant fit parameter.

Summarizing, in case of axisymmetric turbulence there are five adjustable parameters: two exponents $\zeta_2^{(0)}$ and $\zeta_2^{(2)}$ and three prefactors c_0, d_1, d_2. For shear turbulence there is an extra prefactor at $\phi=0$ and a total of seven adjustable parameters for other azimuthal angles. The art is to determine these parameters by fitting the appropriate equation to an experimentally measured structure function.

Rather than finding the best (in a least squares sense) set of parameters, which is a daunting task in seven-dimensional parameter space, we will look for the set of nonuniversal parameters $c_0, d_1, \ldots$ that provide the best fit for given values of the universal exponents $\zeta_2^{(0)}$ and $\zeta_2^{(2)}$. First, the value of the isotropic exponent $\zeta_2^{(0)}$ is guessed, for example, from the transverse structure function G_2^T. Next, the anisotropy exponent $\zeta_2^{(2)}$ is scanned over a range of values. At each $\zeta_2^{(2)}$ we then seek for the nonuniversal constants $c_0, d_1, \ldots$ which minimize the sum of squared differences χ^2 between measurement and fit. The value of this minimum depends on $\zeta_2^{(2)}$, and at some $\zeta_2^{(2)}$ it will be smallest. This distinction between universal and nonuniversal parameters was inspired by Arad *et al.* and Kurien *et al.* [2,6] who followed the same procedure.

TABLE I. Characteristic parameters of the used turbulent flows: (1) axisymmetric turbulence and (2) homogeneous shear turbulence. The mean velocity is U with $u_{rms}=\langle u^2 \rangle^{1/2}$ being the rms size of the fluctuations. For the definition of the other characteristic quantities the rms derivative velocity $\dot{u}_{rms} \equiv \langle (du/dt)^2 \rangle^{1/2}$ is used. For the mean energy dissipation ϵ the isotropic value is taken, $\epsilon = 15\nu \dot{u}_{rms}^2 U^{-2}$ with ν the kinematic viscosity. The Kolmogorov scale is $\eta = (\nu^3/\epsilon)^{1/4}$ and the Taylor microscale is $\lambda = U u_{rms}/\dot{u}_{rms}$ with the associated Reynolds number $Re_\lambda = \lambda u_{rms}/\nu$. The integral length scale is defined in terms of the correlation function of velocity fluctuations $L = \int_0^\infty \langle u(x)u(x+r)\rangle_x dr/\langle u^2 \rangle$. The total integration time T_{int} of the experiment is expressed in integral times by $U T_{int}/L$.

Configuration	U (m/s)	u_{rms} (m/s)	Re_λ	η (m)	L (m)	$U T_{int}/L$
1	10.6	1.14	560	1.6×10^{-4}	0.17	5×10^5
2	11.4	1.15	600	1.6×10^{-4}	0.19	3×10^5

The key question then is if the anisotropy description of measured structure functions enables one to detect the influence of large-scale anisotropy on the shape of the structure function, as characterized by its scaling exponent $\zeta_2^{(2)}$. From dimensional arguments [19] we expect $\zeta_2^{(2)}=4/3$, but the precise value may be influenced by intermittency.

An alternative approach to detect large-scale anisotropy is to measure correlations of the velocity field that vanish exactly in the isotropic case; these correlations and their angular dependence are then determined by anisotropy alone. Mixed structure functions $G_{x\beta}(r e_x)$ were measured in a turbulent boundary layer by Kurien and Sreenivasan [20] using an interpolation scheme to extract an anisotropy exponent. Although such a flow is not only anisotropic but also highly nonhomogeneous, Kurien and Sreenivasan [20] found an anisotropic scaling exponent $\zeta_2^{(2)} \approx 1.21$, which is close to the dimensional estimate $\zeta_2^{(2)}=4/3$. The procedures used also allowed one to find scaling exponents of higher-order mixed structure functions. Similar values of these exponents were also found in homogeneous shear turbulence [21].

In this paper we will analyze experiments involving two turbulent flows with decreasing symmetry. In the first case the flow has axisymmetry, in the second case we consider homogeneous shear turbulence. In both cases turbulence was created in a windtunnel using special grids. These grids were designed to preserve the homogeneity of the flow: the SO(3) description deals with *homogeneous* anisotropic flows. This severe constraint limited the Reynolds number to $R_\lambda \approx 600$. The flow parameters are listed in Table I.

In the following two sections we will describe the two experiments and the analysis of second-order structure functions using the SO(3) formulas Eqs. (3)–(6). We will then consider the angle dependence of third- and seventh-order structure functions in homogeneous shear turbulence.

III. AXISYMMETRIC TURBULENCE

In view of the SO(3) picture, it is attractive to study axisymmetric turbulence as it involves the simplest expression for the angle-dependent structure functions with the smallest number of adjustable parameters. The experimental setup is sketched in Fig. 3 and the flow characteristics are summarized in Table I. Axisymmetric turbulence is generated in the wake of a circularly symmetric target-shaped grid (diameter

0.7 m) placed in a recirculating windtunnel. Velocity fluctuations $u(y)$ are measured 2 m downstream using an array of hot-wire sensors. In all experiments reported here we used probes with a sensitive length of 200 μm. They were operated by a computerized constant temperature anemometer. The velocity signals were low pass filtered at 10 kHz and sampled synchronously at 20 kHz which is approximately twice the Kolmogorov frequency. Each experiment was preceded by a calibration procedure in which the voltage to air velocity conversion for each probe was measured using a calibrated nozzle. The resulting ten calibration tables were updated regularly during the experiment to allow for a (small) temperature increase of the air in our recirculating windtunnel. Statistical convergence was assured by collecting data for several hours (at least 3×10^5 large eddy turnover times).

By time delaying the signals from the wires, the θ dependence of structure functions can be measured. By rotating the entire array along the x axis, the angle ϕ was changed. It was
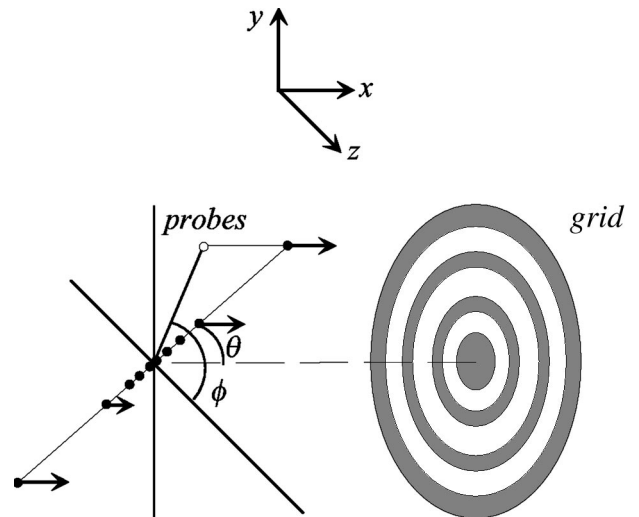

FIG. 3. Axisymmetric turbulence is generated with a target-shaped grid. The orientation of the vector r over which velocity increments are measured is determined by the angles θ and ϕ. The azimuthal angle ϕ is varied by physically rotating the probe array; the polar angle θ is adjusted by varying the time delay between samples, as illustrated in Fig. 1. The characteristics of the flow are listed in Table I. The grid is not drawn to scale.
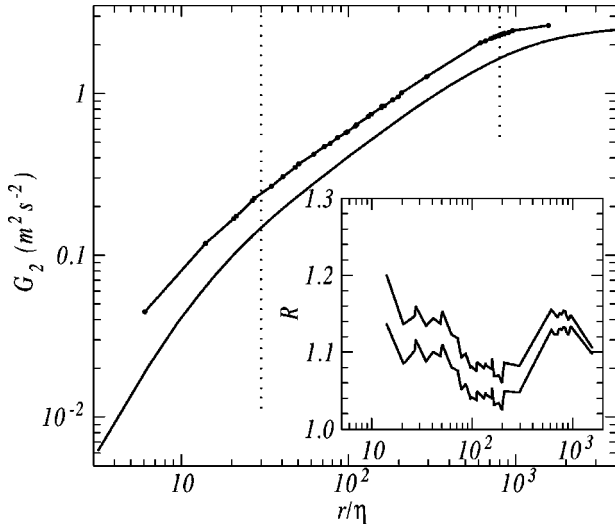
FIG. 4. Longitudinal and transverse structure functions in axisymmetric turbulence. Dots connected by lines, transverse $G_2^T(r)$; line, longitudinal $G_2^L(r)$. The dotted lines indicate the extent of the inertial range. Inset: anisotropy ratio $R(r)$ computed from the longitudinal and transverse structure functions according to Eq. (7). The lower curve assumed the mean velocity as the convection velocity in the Taylor frozen turbulence hypothesis; the upper curve follows the definition of [6].

FIG. 5. Energy spectra of all ten probes of the probe array, which spans a separation of 0.24 m.

verified that all results were independent of ϕ, thus proving the axisymmetry of the flow.

Figure 4 shows the second-order transverse and longitudinal structure functions. The longitudinal structure function is the result of single-probe measurements, translating time delays into spatial separations using Taylor's hypothesis. In a homogeneous flow the longitudinal structure functions measured at the different locations y_i, $i=1,\ldots,10$ of the probes should all be the same.

There are several circumstances which may affect homogeneity: the turbulence properties may depend on y, or the probe array *itself* may influence the measurement in an inhomogeneous fashion. The position of the ten probes was chosen so as to space the 45 distances between them as close as possible to exponential. This causes the probes to crowd near the center two probes which have the smallest separation. At this location one might suspect an influence of the denser detection array on the measured turbulence properties. That this is not the case is demonstrated in Fig. 5 which shows the frequency spectra $E(f,y_i)$ at each probe position y_i; they appear to be virtually independent of y_i. A further proof of the homogeneity of the measured velocity fluctuations is provided by the transverse structure function itself.

We recall that the transverse structure function G_2^T is measured using the discrete distances between probe pairs in the array. Each point of the transverse structure function in Fig. 4, therefore, corresponds to a distance $r=y_i-y_j$ between different probe pairs that are at different locations y_i, y_j. Homogeneity shows in the smoothness of the dependence on the separation r of the transverse structure function. Of course, since the different points of the curve correspond to different probe pairs whose characteristics may be slightly
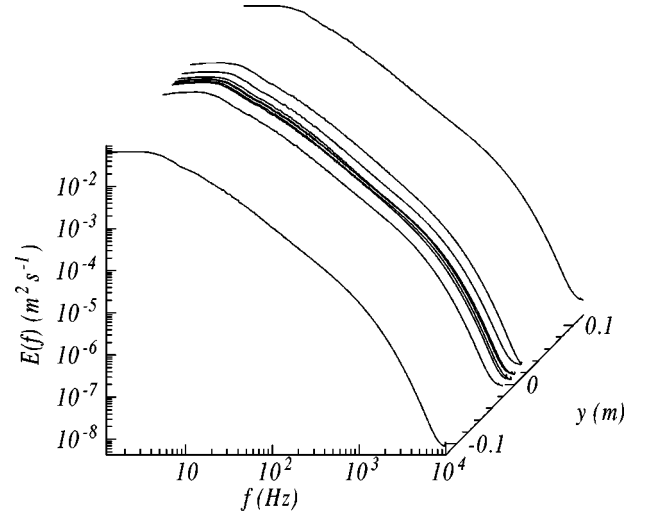
different, the noise in the measured transverse structure functions is larger than in the longitudinal structure functions. We conclude that our flow is axisymmetric and homogeneous, so that the simplest SO(3) decomposition formula Eq. (3) applies which has only three adjustable nonuniversal constants.

The anisotropy of our flow can be learned from the satisfaction of the isotropy relation between measured longitudinal G_2^L and transverse G_2^T structure functions. The relation is such that the anisotropy ratio $R(r)$, which is defined as

$$R(r) \equiv G_2^T(r) \Big/ \left\{ G_2^L + \frac{r}{2} \frac{dG_2^L}{dr} \right\}, \qquad (7)$$

should be identically equal to 1. Satisfaction of $R(r)=1$ can be tested even if scaling behavior is absent. In case of a pure algebraic behavior of one of the structure functions, $R(r)=1$ trivially implies the same algebraic behavior of the other one. In the context of the SO(3) description, where anisotropy is reflected in a mixed algebraic behavior, $R(r)=1$ can accidentally be satisfied in the anisotropic axisymmetric case, but only if a very special relation exists between the parameters $\zeta_2^{(0)}$, $\zeta_2^{(2)}$, c_0, d_1, and d_2 of Eq. (3), which we deem extremely improbable.

So far, experimental studies involving Eq. (7) have used cross wires which measure the u and v velocity components in a point while for both components Taylor's hypothesis is invoked to translate time into space. This is not so for the results shown in Fig. 4, where the transverse structure function uses true spatial separations. Another difference with the cross-wire test is that in our experimental setup $R(r)$ becomes trivially 1 at integral scales since both $G_2^T(r\rightarrow\infty)=G_2^L(r\rightarrow\infty)=2\langle u^2\rangle$. Therefore, $R(r)$ is only sensitive to anisotropy at inertial-range scales. The inset of Fig. 4 shows that $R(r)$ indeed shows a maximum at large scales, with $R=1$ only reached at $r/\eta \gtrsim 2\times10^3$, which is larger than the size of the probe array.

A point of discussion raised in Ref. [6] is whether the true spatial separations r in the transverse structure function G^T

should be related to time-delayed separations $r = U\tau$ of the longitudinal G_2^L using the mean velocity U as the frozen turbulence convection velocity. For their atmospheric boundary layer flow they instead proposed to take $[U^2 + (3u)^2]^{1/2}$ as convection velocity. Because their fluctuation velocity was large ($u/U \approx 0.25$), it raised the convection velocity by 25%. In our case $u/U \approx 0.1$, and as the inset of Fig. 4 shows, the effect on the measured anisotropy is small. What is perhaps important is that the Taylor hypothesis is increasingly challenged at high frequencies (small scales) [22]. This is responsible for the slight increase of $R(r)$ at small scales ($r/\eta \approx 20$). The apparent increase of the anisotropy at small scales is inconsequential for the analysis of the large-scale anisotropy.

The question now is if we can detect the influence of anisotropy at large scales with help of the SO(3) machinery Eq. (2), in particular whether we can recover the anisotropy scaling exponent $\zeta_2^{(2)} = 4/3$ from the behavior of $G_2(r,\theta)$ at large r. First, we measured the angle dependence of G_2 using only two probes spaced at $r_0/\eta = 100$, which is centered in the inertial range $r/\eta \in [30,800]$. The experiment and fit of Eq. (3) are shown in Fig. 6(a). For the fit, we fixed $\zeta_2^{(0)}$ and determined the constants c_0, d_1, d_2 and the exponent $\zeta_2^{(2)}$ in a least squares procedure. The exponent $\zeta_2^{(0)}$ varies from $\zeta_2^{(0)} = 0.70$ to $\zeta_2^{(0)} \approx 0.74$ for the transverse and the longitudinal case, respectively. We select $\zeta_2^{(0)} = 0.72$, and discuss the influence of this particular choice below. Strikingly, the isotropic contribution $r^{\zeta_2^{(0)}} g_0(\theta)$ alone does not provide a satisfying fit, and it is necessary to include the anisotropic contribution. We find that the best fit is reached if $\zeta_2^{(2)} = 1.5$, which is close to the value $4/3$ following from dimensional arguments. The almost perfect fit corresponds to a well-defined minimum of the sum of squared differences χ^2 as shown in Fig. 6(b) where we determined the minimum squared error over a range of $\zeta_2^{(2)}$. As we do not have an independent estimate of the error of measured structure functions, we normalize the minimum χ^2 to 1 by multiplication with an appropriate factor.

These findings completely agree with those of Arad *et al.* and Kurien *et al.* [2,6] who followed a similar procedure in the atmospheric boundary layer and concluded that $\zeta_2^{(2)} = 1.39$. However, repeating the experiment with different probe separations r_0 confuses the issue. As Fig. 6(b) illustrates, the value of $\zeta_2^{(2)}$ that optimizes the fit depends strongly on r_0; it is large ($\zeta_2^{(2)} = 1.8$) at small r_0 and small ($\zeta_2^{(2)} = 1.2$) at large r_0, with both values of r_0 in the inertial range. However, the value $r_0/\eta = 100$ is preferred as it provides the best defined minimum. Such a preference can perhaps be justified by the observation that the angle θ varies most rapidly near $r = r_0$, so that r_0 needs to be chosen well inside the inertial range. In principle, a two-point measurement would suffice to determine the parameters of the SO(3) description, but now the experimental information comes as a single function with a coupled dependence on r and θ. This single function must then be used to determine four unknown parameters. The dependence of the outcome on r_0 indicates that this information is not enough.
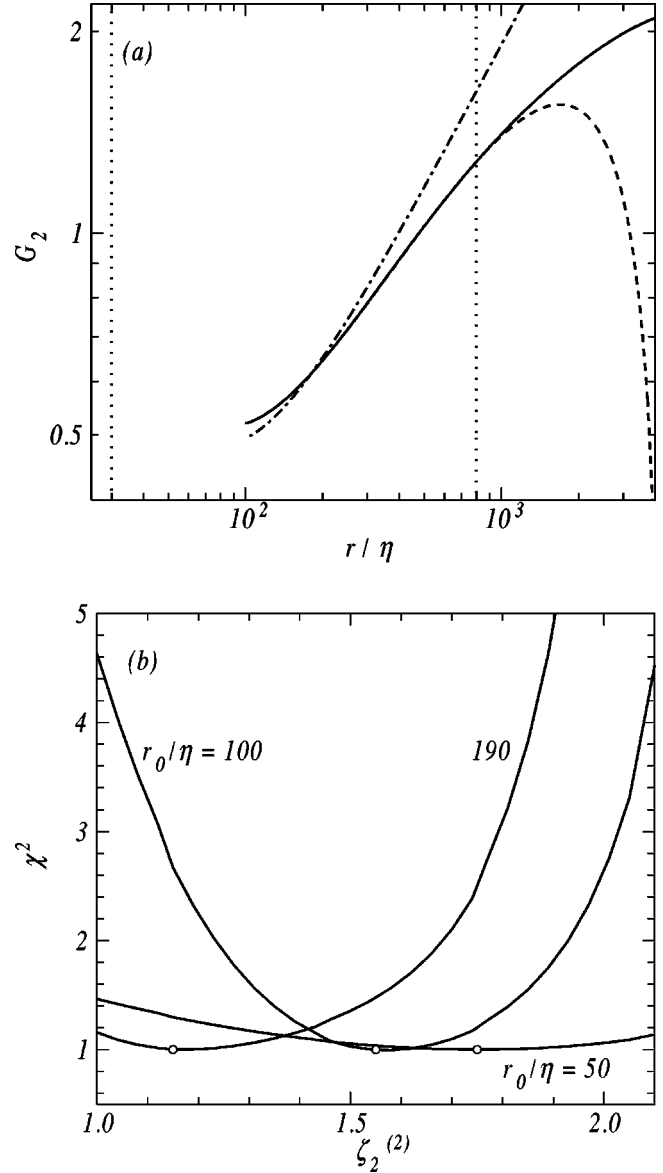

FIG. 6. (a) Full line: measured $G_2(r,\theta)$ using two probes separated at $r_0/\eta = 100$, so that $\theta(r) = \sin^{-1}(r_0/r)$. Dash-dotted line: fit that only includes isotropic part involving $g_0(\theta)$ [Eq. (3)]. Dashed line: fit including both isotropic and anisotropic part. Dotted lines: extent of inertial range. (b) Minimum of the sum of squared differences between measurement and fit for variation of the nonuniversal parameters c_0, d_1, and d_2 at $r_0/\eta = 50$, 100, and 190. The values of $\zeta_2^{(2)}$ that give the best fit are indicated by the open balls. The sum of squared diffences is normalized such that its minimum is always at $\chi^2 = 1$.

The information obtained on the θ dependence of the structure function is greatly enhanced if the number of velocity probes is made large enough such that structure functions at $\theta = 90°$ can be made of pure spatial separations. Measured structure functions $G_2(r,\theta)$ for the pure longitudinal arrangement $\theta = 0$ using time delays only, for $\theta = 15°$, $35°$, $55°$ using a combination of space and time delays, and for the transverse arrangement are shown in Fig. 7. To more clearly expose the quality of the fits, we plot the structure functions compensated by the self-similar behavior
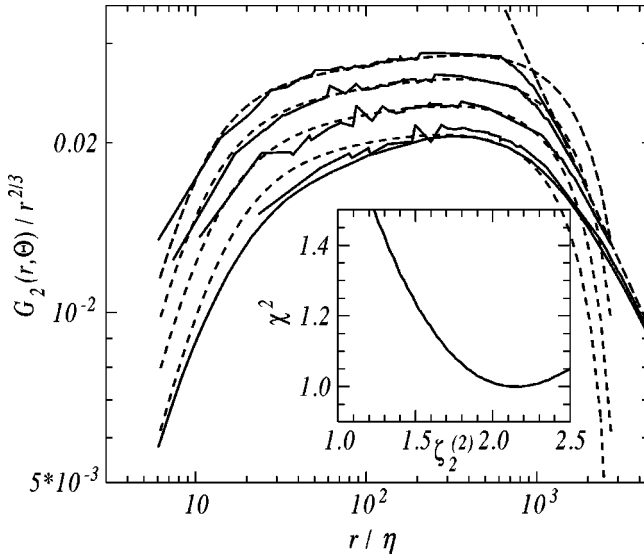
FIG. 7. Full lines measured $r^{-2/3}G_2(r,\theta)$ at $\theta=0$, 15°, 35°, 55°, and 90°. Dashed lines: simultaneous fit of Eq. (3) to the data at $\theta=0°$, 35°, 55°, and 90°. The asymptote of the structure functions $2\langle u^2 \rangle$ is indicated. Inset: minimum of the sum of squared differences between measurement and fit for variation of the the nonuniversal parameters c_0, d_1, and d_2. A minimum is reached at $\zeta_2^{(2)}\approx 2.1$. The sum of squared differences is normalized such that its minimum is always at $\chi^2=1$.

$G_2(r,\theta)\sim r^{2/3}$. This procedure amplifies the noise in the $\theta > 0$ multiprobe structure functions, which is caused by slight differences in probe characteristics. Because the longitudinal structure function at $\theta=0$ is made from time delays only, this curve is smooth. However, the consistency between the single-probe and multiprobe measurements shows in the closeness of the curves at $\theta=0$ and $\theta=15°$.

We have attempted to simultaneously fit the measured structure functions at $\theta=0°$, 35°, 55°, and 90° using Eq. (3) with a single set of parameters; the result is shown in Fig. 7. In correspondence with Fig. 6, the fit range $[r_1, r_2(\theta)]$ was taken from $r_1/\eta=100$ to values $r_2(\theta)$ where $G_2(r,\theta)$ have reached nearly their asymptotic value $\xi 2\langle u^2 \rangle$, with $\xi=0.9$. The small-r dissipative range behavior was modeled by replacing the isotropic part in Eq. (3) by

$$c_0\left\{ h(r) + \sin^2(\theta)\frac{r}{2}\frac{dh}{dr} \right\}$$

with $h(r)=r^2(1+(r/r_c)^2)^{(\zeta_2^{(0)}-2)/2}$ (8)

and $r_c/\eta=12.6$. The function $h(r)$ [23,24] models the transition from dissipative scales, $h(r)\sim r^2$, to inertial-range scales, $h(r)\sim r^{\zeta_2^{(0)}}$. This choice improves the appearance of the fit, but it is completely inconsequential for our conclusions.

Using a single set of parameters it is possible to obtain a satisfactory fit of $G_{xx}(r,\theta)$ over the indicated fit range and at all θ, except perhaps at $\theta=0$ where the large-scale behavior of the longitudinal structure function is not represented properly. However, the variation with θ is mostly due to the

(trivial) θ dependence of g_0. At $r/\eta=10^3$ the relative size of the anisotropic part, $r^{\zeta_2^{(2)}-\zeta_2^{(0)}}g_2(\theta)/g_0(0)$, ranges only from -0.21 at $\theta=\pi/2$ to -0.22 at $\theta=0$. Although such slight dependence on θ could still be compatible with the SO(3) description, it complicates the measurement of the anisotropy scaling exponent $\zeta_2^{(2)}$.

Also in this case, we find a poorly defined minimum of the sum of squared differences χ^2 at a value of the anisotropy exponent $\zeta_2^{(2)}\approx 2.1$ which is much larger than the dimensional prediction $\zeta_2^{(2)}=4/3$. A serious problem is that the position of the minimum strongly depends on the assumed value of $\zeta_2^{(0)}$, it varies from $\zeta_2^{(2)}=2.5$ at $\zeta_2^{(0)}=0.70$ to $\zeta_2^{(2)}=2.0$ at $\zeta_2^{(0)}=0.74$.

Trivially, all second-order structure functions reach at large r the asymptote $G_2(r,\theta)\rightarrow 2\langle u^2 \rangle$; this asymptote is also shown in Fig. 7. The SO(3) description applies to the r dependence of the structure function *before* this asymptote is reached, a dependence which varies in a characteristic way with the angle. This is a subtle point because we always find $g_2(\theta)<0$, which may also represent the trivial rise to saturation of the structure function.

We conclude that for our axisymmetric turbulence the two-probe experiment gives insufficient information to test the SO(3) description. The more extended information that is contained in a full r,θ dependence of the structure function shows that in this case an anisotropy exponent $\zeta_2^{(2)}$ cannot be determined unambiguously.

IV. SHEAR TURBULENCE

While the anisotropy of the axisymmetric turbulence of Sec. III may be modest, a much stronger angle dependence was created in homogeneous shear turbulence. Homogeneous shear turbulence has a linear variation of the mean flow velocity U in the shear direction, a constant fluctuation velocity u, and an energy spectrum that does not depend on y. It is the simplest possible anisotropic turbulent flow, whose large-scale anisotropy is characterized by a single number: the shear rate $S=dU/dy$. Whilst the anisotropy is stronger, the SO(3) description now also has more adjustable parameters due to the loss of symmetry.

To generate a uniform mean velocity gradient we use a grid (dimension 0.9×0.7 m^2) whose y dependent solidity is tuned to preserve a constant turbulence intensity u throughout most of the windtunnel height. The experimental arrangement is sketched in Fig. 8. With the mean flow $U(y)$ in the x direction, the shear points in the transverse y direction. The challenge of the experiment is to maintain the homogeneity of the flow: the SO(3) theory [Eq. (2)] describes anisotropy but presupposes homogeneity. That this challenge is met in our experiments is illustrated in Fig. 9(a) which shows the variation of the mean flow and the turbulence intensity with y. It is seen that the mean velocity profile is linear, with a small variation of the turbulence intensity over the probe array. Further evidence of homogeneity is provided by Fig. 9(b), which shows that the energy spectra, and thus all second-order quantities, such as the integral scale L, do not vary significantly with y.
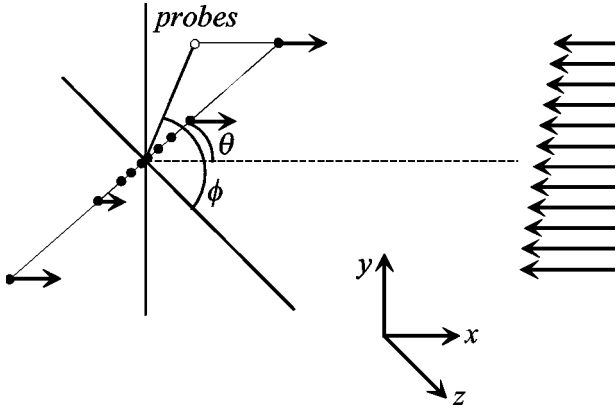
FIG. 8. Homogeneous shear is generated using a grid with variable solidity. The mean velocity increases in the y direction, but is does not vary with z. The (effective) orientation of the probe array is determined by the angles θ and ϕ.

In this flow, the structure function depends both on θ and ϕ, and we measured first the θ dependence at $\phi = \pi/2$. Due to the absence of both axisymmetry and the partial θ symmetry at $\phi = 0$, the general expression Eq. (5) has to be used with five nonuniversal parameters. The result of a fit of this formula to the measured structure function, using a single set of parameters, is shown in Fig. 10. In comparison to the case of axisymmetric turbulence (Fig. 7) the larger number of parameters gives a better fit at angles θ close to the transverse $\pi/2$, but in both cases angles close to the longitudinal ones, $\theta = 0$, are not represented well by the fit. Surprisingly, the best fit now occurs at $\zeta_2^{(2)} \approx 1.3$ which is very close to the dimensional prediction $\zeta_2^{(2)} = 4/3$. Contrary to the axisymmetric flow, the assumed value of $\zeta_2^{(0)}$ now hardly affects the minimum $\zeta_2^{(2)}$.

In contrast to the experiment in axisymmetric turbulence, the anisotropic contribution shows a significant variation with the angle θ. At $r/\eta = 10^3$ the relative size of the anisotropic part, $r^{\zeta_2^{(2)} - \zeta_2^{(0)}} g_2(\theta)/g_0(0)$, now ranges from -0.36 at $\theta = \pi/2$ to -0.28 at $\theta = 0$. It is precisely this angular variation that is the hallmark of the SO(3) description, and which must be used to determine the anisotropy scaling exponent. That we now find a value of $\zeta_2^{(2)}$ which is closer to the dimensional value 4/3 may be due to the larger variation with θ of the anisotropic contribution.

For the axisymmetric turbulent flow we have verified that there is no ϕ dependence, as it should. For shear turbulence, instead, a clear ϕ dependence of the second-order structure function is expected, given the strong asymmetry of the flow. We therefore measured the structure function $G_2(r, \theta = \pi/2, \phi)$ as a function of ϕ by rotating the probe array. According to Eq. (6), the SO(3) analysis predicts a ϕ dependence

$$G_{xx}(r, \phi) = g_0 r^{\zeta_2^{(0)}} + D(\phi) r^{\zeta_2^{(2)}}, \qquad (9)$$

with $D(\phi) = d_5 + d_6 \cos(2\phi)$, and the variation with ϕ of the anisotropic contribution would be largest if the azimuthal angle is rotated from $\phi = 0$ (perpendicular to the shear) to
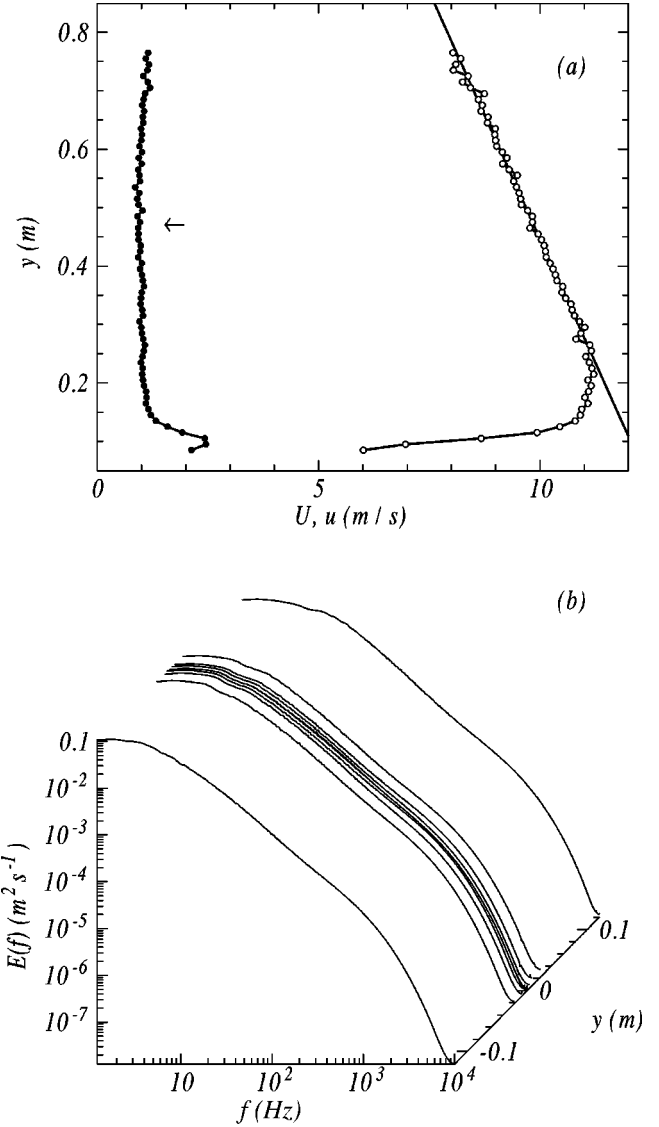

FIG. 9. Homogeneous shear turbulence. (a) Open circles, mean velocity U; closed dots, rms fluctuations u at $x/H = 5.1$ behind the shear generating grid, where $H = 0.9$ m is the height of the tunnel. Near the lower wall the turbulent boundary layer marks the end of the homogeneous shear region. The shear strength is $dU/dy = 5.95$ s^{-1}. (b) Variation of the spectra over the extent (0.24 m) of the probe array. The point $y = 0$ indicates the center of the probe array; it is aligned with the arrow, the center of the shear profile, in frame (a).

$\phi = \pi/2$ (along the shear). This of course also follows from the r-reflection symmetry of the second-order structure function.

Compensated structure functions $r^{-2/3} G_2(r, \theta = \pi/2, \phi)$ for these two angles are shown in Fig. 11. Let us emphasize that these measurements do not involve invocation of Taylor's frozen turbulence hypothesis. A disadvantage of the physical rotation, however, is that the curves have larger fluctuations at large r due to a slight inhomogeneity of the flow. Instead of extracting the anisotropy exponent $\zeta_2^{(2)}$, we set $\zeta_2^{(2)} = 4/3$ and extract the angle dependence $D(\phi)$ from the experiment. As is shown in Fig. 11, the found angular
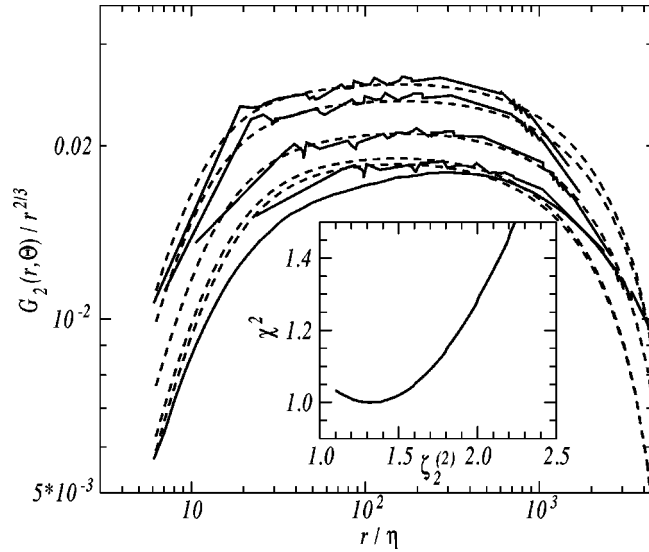
FIG. 10. Full lines measured $r^{-2/3}G_2(r,\theta)$ at $\theta=0$, 15°, 35°, 50°, and 90°. Dashed lines: simultaneous fit of Eq. (5) to the data at $\theta=0°$, 15°, 35°, 50°, and 90°. The asymptote of the structure functions $2\langle u^2\rangle$ is indicated. Inset: minimum the of sum of squared differences between measurement and fit for variation of the five nonuniversal parameters c_0, d_1, d_2, d_3, and d_4. A minimum is reached at $\zeta_2^{(2)}\approx 1.3$. The sum of squared differences is normalized such that its minimum is always at $\chi^2=1$.

dependence of $D(\phi)$ is indeed very close to that of $\cos(2\phi)$. Clearly, the reflection symmetry of G_2 dictates a ϕ dependence such as $\cos(2n\phi)$, but it is remarkable that the measured $D(\phi)$ is actually so close to $\cos(2\phi)$.

Representations of the structure function that resemble Eq. (9), but which are not identical to it, also produce a
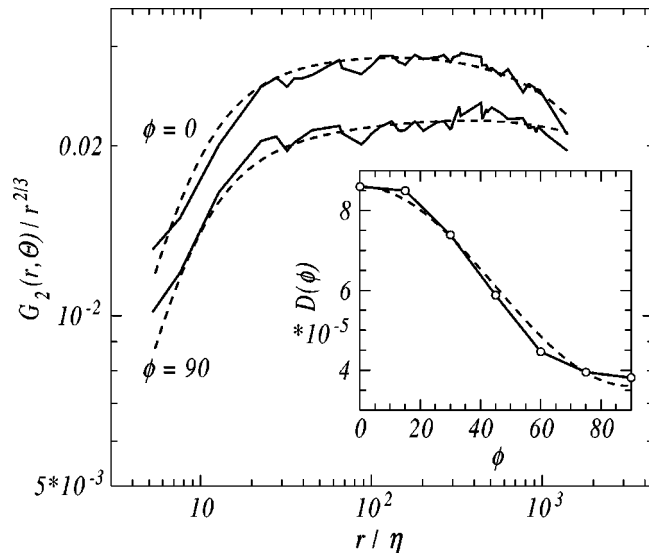

FIG. 11. Azimuthal dependence of structure functions in shear turbulence. Full lines: measured $r^{-2/3}G_2(r,\theta,\phi)$ at $\theta=\pi/2$ and $\phi=0°$, and 90°. Dashed lines: fits of Eq. (9). For clarity, the curves at $\phi=0°$ have been multiplied by a factor 1.2. Inset: open balls, function $D(\phi)$ determined from fits at seven ϕ angles, dashed line, fit of $d_5+d_6\cos(2\phi)$.

similar ϕ dependence. For example, we have modeled the manner in which $G_2(r,\phi)$ reaches its large-r asymptote $2\langle u^2\rangle$ as

$$G_2(r,\phi)=ar^{\zeta_2^{(0)}}[1+r/L(\phi)]^{-\zeta_2^{(2)}},$$

and found a similar $\cos(2\phi)$ dependence of $L(\phi)$ over the r dynamical range of the experiment.

In conclusion, for our experiment on homogeneous shear turbulence, the SO(3) machinery appears to work: We were able to extract the anisotropy exponent from the polar angle dependence of the second-order structure function. Conversely, we have shown that its azimuthal dependence is according to the first anisotropic sector.

V. HIGHER-ORDER STRUCTURE FUNCTIONS

As was realized earlier [20], a better approach to quantify anisotropy may be to measure structure functions whose isotropic part vanishes. Since we measure only one velocity component, the lowest-order tensorial quantity that does so is the third-order structure function

$$G_{\alpha\alpha\alpha}(\mathbf{r})\equiv\langle[u_\alpha(\mathbf{x}+\mathbf{r})-u_\alpha(\mathbf{x})]^3\rangle, \quad (10)$$

with $\alpha=x$ in our case. This tensor quantity can also be expanded in irreducible components.

$$G_{\alpha\alpha\alpha}=g_0^3(\theta)r+g_2^3(\theta,\phi)r^{\zeta_3^{(2)}}+\cdots, \quad (11)$$

where the superscript 3 on $g_{0,2}$ now indicates the order. However, while incompressibility of the velocity field reduces the number of unknown parameters of the anisotropic part of the *second-order* structure function g_2^2 to just a few, no such reduction for g_2^3 is possible, unless the statistical properties of the driving force (the velocity-pressure correlations) are known. The well-known von Kármán–Howarth–Kolmogorov equation fixes the isotropic component

$$g_0^3(\theta)=-\tfrac{4}{5}\epsilon\cos(\theta). \quad (12)$$

In the case of isotropic turbulence, a relation similar to Eq. (7) exists for the third-order angle-dependent structure function $G_{xxx}(r,\theta)$ in terms of the longitudinal structure function $G_3^L(r)\equiv G_{xxx}(r,\theta=0)$:

$$G_{xxx}(r,\theta)=\tfrac{1}{2}\cos\theta\left\{[1+\cos^2(\theta)]G_3^L(r)\right.$$
$$\left.+\sin^2(\theta)r\frac{d}{dr}G_3^L(r)\right\}. \quad (13)$$

In axisymmetric turbulence it follows from reflection symmetry that $G_{xxx}=0$ at $\theta=\pi/2$, which trivially applies to the isotropic part Eq. (12), but also to the anisotropic part. Using multiprobe arrays, it is possible to measure G_{xxx} at small angles θ, but it poses extreme requirements on probe calibration as pairs of probes must now be sensitive to slight asymmetries between positive and negative velocity increments.
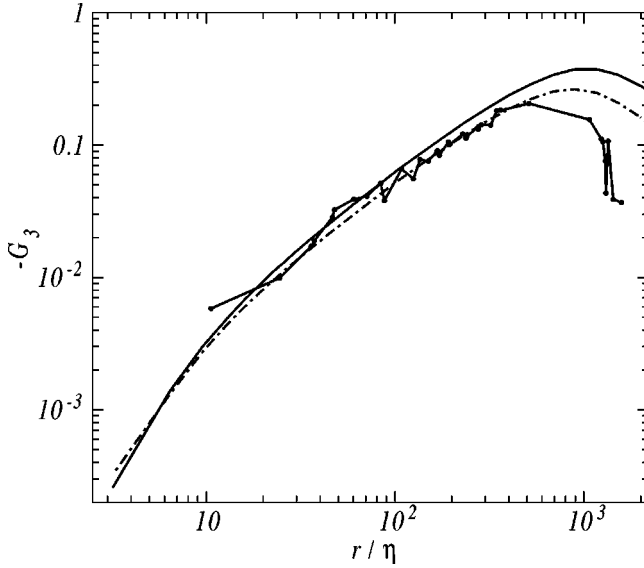
FIG. 12. Third-order structure function measured in axisymmetric turbulence. Full line: longitudinal structure function G_3^L at $\theta = 0$. Dots connected by lines, $G_{xxx}(r,\theta)$ at $\theta = 35°$; dash-dotted line, $G_{xxx}(r,\theta)$ computed from G_3^L using the isotropy relation Eq. (13).

Figure 12 shows the longitudinal $G_3^L(r)$ which was measured using time delays and $G_{xxx}(r,\theta)$ at $\theta = 35°$, together with the isotropic prediction Eq. (13). Clearly, it is not possible in axisymmetric turbulence to distinguish the measured curve at $\theta = 35°$ from the isotropic prediction and it is therefore not possible to deduce information about an anisotropic contribution. Third-order transverse structure functions were also measured in [20] in (inhomogeneous) boundary-layer turbulence. However, in this case the structure function was computed from the absolute values of the velocity increments $\langle |\Delta u|^3 \rangle$, for which a decomposition Eq. (11) is very troublesome as it can never involve the proper isotropic part.

In shear turbulence, the reflection symmetry $\theta \leftrightarrow \pi - \theta$ is broken at $\phi \neq 0$ and the anisotropic part is no longer bound to vanish at $\theta = \pi/2$. Angle-dependent third-order structure functions are shown in Fig. 13(a) for angles $\phi = \pi/2$ and $\theta = 0$ (longitudinal), $\theta = 15°, \theta = 35°$, and $\theta = 60°$. In this case the isotropic contribution vanishes at $\theta = \pi/2$, and only the anisotropic contributions remain. If higher-order anisotropies with $l > 2$ are absent, the scaling at $\theta = \pi/2$ would be pure and the scaling at smaller angles would be a mixture. The scaling exponent at $\theta = \pi/2$ can then be identified with $\zeta_3^{(2)}$; we find $\zeta_3^{(2)} \approx 1.4$, which is significantly larger than the isotropic exponent $\zeta_3^{(0)} = 1$, and is rather close to the dimensional prediction $\zeta_3^{(2)} = 5/3$. If the SO(3) description applies, the scaling of the longitudinal structure function would be a mixture of both exponents

$$G_3^L = -\frac{4}{5}\epsilon r + b r^{\zeta_3^{(2)}}, \qquad (14)$$

with $\zeta_3^{(2)} \approx 1.4$. Figure 13(b) illustrates that it is possible to find a factor $b > 0$ to describe the behavior of the longitudinal structure function at large scales. The dissipation rate ϵ in
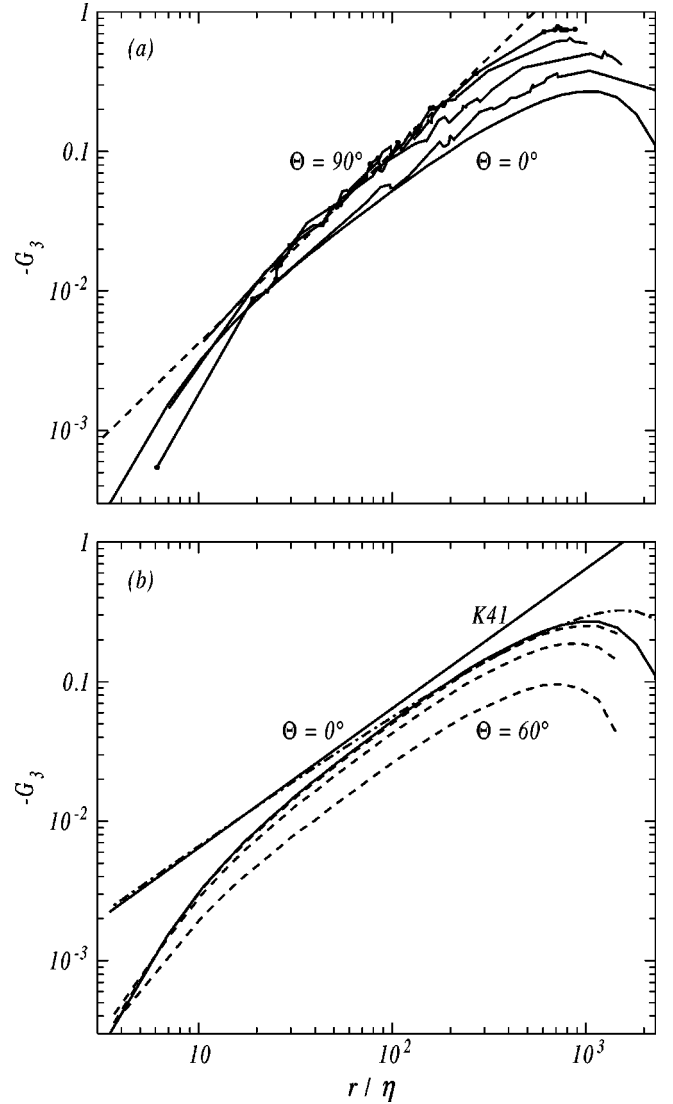

FIG. 13. Third-order structure function measured in homogeneous shear turbulence. (a) Full lines: $G_{xxx}(r,\theta)$ at $\theta = 0°$ (longitudinal), $\theta = 15°$, $\theta = 35°$, $\theta = 60°$, and $\theta = 90°$. Dashed line: fit of $G_{xxx}(r,\theta = 90°) \sim r^{\zeta_3^{(2)}}$, with $\zeta_3^{(2)} \approx 1.4$. (b) Full line: third-order longitudinal structure function. Dashed lines: $G_{xxx}(r,\theta)$ at $\theta = 15°$, $\theta = 35°$, and $\theta = 60°$ computed from the longitudinal one using Eq. (13). The Kolmogorov prediction $G_{xxx}(r,\theta = 0) = -\frac{4}{5}\epsilon r$ is indicated by K41. Dash-dotted line: fit of Eq. (14).

Eq. (14) was estimated from the longitudinal derivative $\epsilon = 15\nu \langle (\partial u/\partial x)^2 \rangle$, with ν being the kinematic viscosity. The admixture of the anisotropic scaling in the longitudinal structure function G_3^L may explain why its apparent scaling exponent is smaller than 1, and why the apparent inertial range of G_3^L is smaller than that of the transverse structure function at $\theta = \pi/2$.

The factor b in Eq. (14) is an unknown function of θ and ϕ which can only be specified in a very general sense in the SO(3) description, using many undetermined parameters. It can, however, in any case be concluded that $b(\theta, \phi = 0)$ must change sign between $\theta = 0$ and $\theta = \pi/2$. This implies that there is an intermediate angle where the scaling is pure iso-
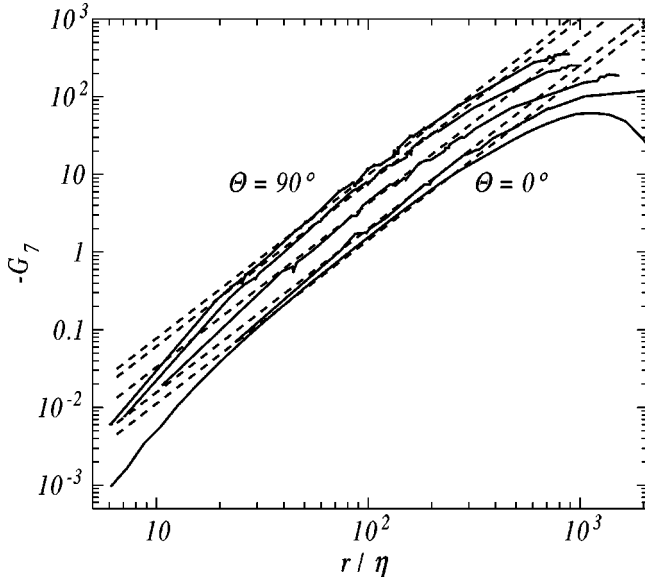
FIG. 14. Seventh-order structure function measured in homogeneous shear turbulence. Full lines: $G_{7(x)}(r, \theta)$ at $\theta = 0°$ (longitudinal), $\theta = 15°$, $\theta = 35°$, $\theta = 60°$, and $\theta = 90°$. Dashed lines: fit of $G_{7(x)}(r, \theta) \sim -[0.9 + 5.2 \sin^2(\theta)] r^{2.1}$.

tropic, with scaling exponent 1. From Fig. 13(a) we estimate this *magic angle* θ_m to be $\theta_m \approx 15°$.

Apparently, the anisotropic contribution to G_3^L ($\theta = 0$) is small. For larger θ the isotropic contribution vanishes according to Eq. (13), in a way that is illustrated in Fig. 13. At the same time, the anisotropic contribution increases, changes sign at $\theta = \theta_m$, and according to Fig. 13(a), grows larger than the isotropic part at $\theta = 0$. Therefore, the amplitude of the θ dependence of the anisotropic $g_2^3(\theta)$ is larger than that of the isotropic $g_0^3(\theta)$. This is contrary to the SO(3) picture, where we would expect the anisotropic part to be (much) smaller than the isotropic part.

In principle, low-order structure functions are affected by intermittency. This was already observed in the value of the scaling exponent $\zeta_2^{(0)}$ which in both flows significantly exceeds the self-similar value 2/3. As intermittency effects are stronger for high orders, we show the angle dependence of $G_{7(x)}(r, \theta)$ in Fig. 14. Contrary to the third order $G_{xxx}(r, \theta)$, the scaling exponent is almost independent of the angle (it varied from 2.1 for $\theta = 0$ to 2.2 for $\theta = \pi/2$). For $r/\eta \lesssim 500$, a satisfactory fit could be obtained through $G_{7(x)}(r, \theta) \sim [0.9 + 5.2 \sin^2(\theta)] r^{2.1}$, where we emphasize the dependence on the *double* angle through $\sin^2(\theta)$. Such a fit is possible because of the relatively small noise in $G_{7(x)}(r, \theta)$. Although its order is higher, the noise in the seventh-order structure function is smaller than that in the third-order one of Fig. 13.

We conclude that for higher orders the θ dependence of structure functions is strongly influenced by intermittency, such that intermittency amplifies anisotropy. For example, it was noticed by us that, unlike the longitudinal exponents, the transverse ones tend to a limiting value at very large orders [25]. Another example is the observation that the hyper skewness $G_{7(x)}(\eta)/G_2^T(\eta)^{7/2}$ does not decay with increasing

Reynolds number [7]. A challenge is to design quantities for unfolding the effects of intermittency and anisotropy. In this respect Ref. [8] shows that anisotropy is still observed at the highest Reynolds numbers obtainable in the laboratory, even when intermittency effects are accounted for. For the second order structure functions studied in this paper, isotropy will eventually be restored at the smallest scales as r^α, with $\alpha = \zeta_2^{(2)} - \zeta_2^{(0)} > 0$.

VI. SUMMARY AND CONCLUSION

The key idea of the SO(3) description is that the observed imprint of anisotropy due to stirring at large scales is dependent on the geometric arrangement of the measurement. At some angles, the effects of anisotropy are larger than at others. The expected angular dependence can be worked out in detail using the formalism of angular momentum theory and can be used in experiments to unfold the effect of anisotropy on measured second-order structure functions.

In this paper we have described several experimental procedures to unfold structure functions using this angular dependence. Second-order structure functions of a single velocity component contain a mixture of isotropic and anisotropic contributions, which makes it difficult to extract the scaling of the anisotropic contribution.

We conclude that it is essential to use measurements of the separate angle and distance dependence of structure functions. For axisymmetric turbulence, the apparent success of a simple two-probe arrangement where distance and angle information are intertwined could not be reproduced when considering the information present in a multiprobe configuration.

At this point we disagree with the conclusions of Arad *et al.*, Kurien *et al.*, and Kurien and Sreenivasan [5,6,26], who analyzed boundary-layer turbulence using a two-probe arrangement. There are several possible explanations for this discrepancy. First, the Reynolds number in the atmospheric boundary layer that was studied in Refs. [5,6,26] is much larger than ours, which may help to separate the effects of large-scale anisotropy on inertial-range scaling. Second, the dependence on the separation r_0 of the probes was not checked in Refs. [5,6,26]. Finally, Refs. [5,6,26] apply the axisymmetric formulas, while boundary-layer turbulence is not axisymmetric The authors argue that in the two-probe method the large separations r (which are most affected by anisotropy) come with small θ. At small θ the functional forms of the axisymmetric angular dependence Eq. (3) and the general formula Eq. (5) are not very different, so that the axisymmetric formula would still be applicable. This again illustrates the necessity of a separate measurement of both angle θ and r dependence of the structure function.

For the more strongly anisotropic shear turbulence the SO(3) machinery to analyze second-order structure functions appears to work, at least our data are consistent with the dimensional value 4/3 of the anisotropic scaling exponent $\zeta_2^{(2)}$ and the dependence on the azimuthal angle ϕ agrees with the predicted $\cos(2\phi)$ angular dependence of the anisotropic sector.

In connection with the $\zeta_2^{(2)} = 4/3$ value of the anisotropy

scaling exponent, a paper by Lumley is often cited [19]. This paper discusses an elaborate scaling theory where the scaling of the anisotropy corrections follows from the requirement that the structure function be analytic in the shear rate S. However, this only predicts the value 4/3 for the *cross*-structure functions G_{xy} and G_{zy} which are proportional to S. On the other hand, G_{xx} would then involve S^2, which dictates the scaling of the anisotropic part to be $\zeta_2^{(2)} = 2$.

For shear turbulence it was possible to isolate the anisotropic contribution in the *third-order* structure function, which turned out to be of the same order of magnitude as the isotropic part. We do not know how to reconcile this finding with the SO(3) picture, where an anisotropic contribution is a *correction*. Further theoretical work on an SO(3) description of higher-order structure functions is clearly needed. For higher-order structure functions, the effects of intermittency become dominant, and an intriguing question is the relation between intermittency and anisotropy.

One could object that the anisotropy of the flows that are considered in this paper is small, and that consequently the anisotropy content of the structure functions is too small to be able to detect the anisotropy scaling exponent. While this may be so for the axisymmetric flow, this is definitely not the case for the homogeneous shear experiment where turbulence properties strongly depend on the direction. In both experiments we strived for homogeneity of the flow, which compromised the achieved anisotropy. Better control of the turbulence, for example through active grids may help to create homogeneous flows that are more strongly anisotropic [7].

Another objection may be that our Reynolds numbers are too small so that there is not a clear separation between inertial-range and integral scales. However, it is generally believed that precisely these moderate Reynolds numbers would benefit most of the SO(3) description. We emphasize that success of this approach was concluded in the case of direct numerical simulations which had a very small Reynold number [17,18].

We conclude that great care is needed to extract the anisotropy according to the SO(3) picture from experiments on strong turbulence. Before we can decide the same success as in numerical simulations [17,18], more experiments are needed. These experiments must involve arrays of probes that can also measure several velocity components. In this way it should be possible to measure the angular dependence of only the anisotropic sector of the second-order structure function.

[1] V. L'Vov, E. Podivilov, and I. Procaccia, Phys. Rev. Lett. **79**, 2050 (1997).

[2] I. Arad, V. L'Vov, and I. Procaccia, Phys. Rev. E **59**, 6753 (1999).

[3] C. Cambon and C. Teissedre, Acad. Sci., Paris, C. R. **301**, 65 (1985).

[4] M. Jones, *Spherical Harmonics and Tensors for Classical Field Theory* (Research Studies Press Ltd., Letchworth, England, 1985).

[5] I. Arad, B. Dhruva, S. Kurien, V. L'Vov, I. Procaccia, and K. Sreenivasan, Phys. Rev. Lett. **81**, 5330 (1998).

[6] S. Kurien, V. L'Vov, I. Procaccia, and K. Sreenivasan, Phys. Rev. E **61**, 407 (2000).

[7] X. Shen and Z. Warhaft, Phys. Fluids **12**, 2976 (2000).

[8] J. Schumacher, K. Sreenivasan, and P. Yeung, Phys. Fluids **15**, 84 (2003).

[9] W. van de Water and J.A. Herweijer, Phys. Scr., T **67**, 136 (1996).

[10] W. van de Water and J.A. Herweijer, J. Fluid Mech. **387**, 3 (1999).

[11] B. Dhruva, Y. Tsuji, and K. Sreenivasan, Phys. Rev. E **56**, R4928 (1997).

[12] S. Grossmann, D. Lohse, and A. Reeh, Phys. Fluids **9**, 3817 (1997).

[13] O. Boratav, Phys. Fluids **9**, 3120 (1997).

[14] S. Chen, K. Sreenivasan, M. Nelkin, and N. Cao, Phys. Rev. Lett. **79**, 2253 (1997).

[15] X. Shen and Z. Warhaft, Phys. Fluids **14**, 370 (2002).

[16] S. Grossmann, D. Lohse, and A. Reeh, J. Stat. Phys. **93**, 715 (1998).

[17] I. Arad, L. Biferale, I. Mazzitelli, and I. Procaccia, Phys. Rev. Lett. **82**, 5040 (1999).

[18] L. Biferale and F. Toschi, Phys. Rev. Lett. **86**, 4831 (2001).

[19] J.L. Lumley, Phys. Fluids **10**, 855 (1967).

[20] S. Kurien and K. Sreenivasan, Phys. Rev. E **62**, 2206 (2000).

[21] See Z. Warhaft and X. Shen, Phys. Fluids **14**, 2432 (2002), in order to distinguish the longitudinal structure function from the cross-structure function which does not have an isotropic part, this paper identifies the longitudinal structure function with the isotropic sector. However, this is not correct, as the longitudinal structure function contains a *mixture* of isotropic and anisotropic contributions.

[22] E. Gledzer, Physica D **104**, 163 (1997).

[23] G. Stolovitzky, K. Sreenivasan, and A. Juneja, Phys. Rev. E **48**, R3217 (1993).

[24] G. Batchelor, Proc. Cambridge Philos. Soc. **47**, 359 (1951).

[25] A. Staicu and W. van de Water, Phys. Rev. Lett. **90**, 094501 (2003).

[26] S. Kurien and K. Sreenivasan, in *New Trends in Turbulence*, edited by M. Lesieur, A. Yaglom, and F. David (Springer-EDP, Paris, 2001), pp. 53–110.